This is an *Accepted Manuscript*, which has been through the Royal Society of Chemistry peer review process and has been accepted for publication.

Accepted Manuscripts are published online shortly after acceptance, before technical editing, formatting and proof reading. Using this free service, authors can make their results available to the community, in citable form, before we publish the edited article. We will replace this *Accepted Manuscript* with the edited and formatted *Advance Article* as soon as it is available.

You can find more information about *Accepted Manuscripts* in the **Information for Authors**.

Please note that technical editing may introduce minor changes to the text and/or graphics, which may alter content. The journal's standard **Terms & Conditions** and the **Ethical guidelines** still apply. In no event shall the Royal Society of Chemistry be held responsible for any errors or omissions in this *Accepted Manuscript* or any consequences arising from the use of any information it contains.

Chem Comm

COMMUNICATION

Localized polyselenides in a graphene-coated polymer separator for high rate and ultralong life lithium-selenium batteries

Ruopian Fang, Guangmin Zhou, Songfeng Pei, Feng Li* and Hui-Ming Cheng

A graphene-coated polymer separator was developed for lithium-selenium batteries with pure selenium powder as the active material. The structure is a simple yet effective strategy for improving Li-Se battery electrochemical performance, yielding long cycle up to 1000 cycles with high capacity and excellent rate behavior.

Rechargeable batteries with high energy density, long cycle life and low cost are of great importance to meet the ever increasing demands for electrochemical energy storage applications.[1-3] However, the state-of-the-art rechargeable batteries with lithium intercalation compounds as cathode materials have limited capacities.[4, 5] As a result, the discovery of high-energy cathode materials is crucial for electrochemical energy storage systems. Recently, tremendous attention has been given to lithium-sulfur (Li-S) batteries due to their intrinsic virtues including high theoretical specific energy density (2567Wh kg^{-1}) and low cost.[3, 6-11] However, the development of Li-S batteries has been impeded by the intrinsic drawbacks of sulfur such as its insulating nature.[8] Therefore, it is of great importance to explore other desirable high-energy battery systems.

In this regard, selenium, which is next to sulfur in the VIA group in the periodic table, has been considered because it shows similar chemical properties to sulfur. Selenium has a theoretical gravimetric capacity of 678 mAh g^{-1} and a high theoretical volumetric capacity of 3253Ah L^{-1} comparable to that of sulfur (3467Ah L^{-1}) due to its higher density (2.5 times that of sulfur). Generally, volumetric energy density is particularly important when battery packages for portable electronic devices or EVs must be installed in a limited space. Additionally, the electronic conductivity of selenium (1×10^{-3} S m^{-1}) is significantly higher than that of sulfur (5×10^{-28} S m^{-1}), and a recent report showed that lithiated selenium (Li$_2$Se) might be more conductive than lithiated sulfur (Li$_2$S),[12] indicating that selenium possesses higher electrochemical activity. Therefore, as another electrochemically active material that, like sulfur, can accept up to two electrons per atom, selenium is also a prospective candidate for high energy cathode materials.[13] However, unlike conventional intercalation cathode materials, both sulfur and selenium undergo a series of compositional and structural change during cycling,[7, 14] which involve the dissolution of intermediate

polysulfides/polyselenides (Li$_2$S$_x$/Li$_2$Se$_x$, $3 \leqslant x \leqslant 8$) and thus cause an irreversible capacity loss and the known "shuttle effect".[6-9, 14] The extensive efforts have been devoted to trapping the polysulfides by encapsulating sulfur in various porous carbons,[15] graphene materials[10, 16] or conductive polymers.[17] On the other hand, adding a barrier layer such as a carbon coating that can effectively absorb polysulfides between the cathode and separator can also greatly improve the performance of Li-S batteries.[9, 18, 19] For example, our group previously showed the greatly improved performance of a Li-S battery with a graphene membrane as current collector and a graphene coating on a polymer separator.[9, 19] As for Li-Se batteries, one typical strategy to achieve higher performance of the Se cathode is impregnating Se into various porous carbon matrixes, which usually involves complex multi-step processes.[12, 20-25] Although good cyclic stability has been demonstrated, it should be noted that in most work a large amount of porous carbon is used, leading to low Se contents in the final cathodes (less than 62%),[12, 20-25] and the carbonate-based electrolyte used in these composites was not compatible with open-type high Se-loaded cathodes.[21] There is no doubt that the overall energy density of Li-Se batteries would be seriously reduced with the use of these low Se content cathodes. Therefore, simultaneous realization of a high Se content and excellent electrochemical performance still remains a great challenge.

Here we explore the pure selenium powder as an active material without involving any complex fabrication process. The weight of Se in the final electrode is 70%, which is the highest value reported to date.[12, 20-25] Specifically, graphene was coated on a commercial polymer separator and acted as a barrier layer between the cathode and separator. This design enables the achievement high-performance Li-Se batteries with a high Se content.

An illustration of a Li-Se cell with a graphene-coated polymer separator (graphene-polymer separator) is shown in Fig. 1a, and the graphene side (black) faces the Se cathode. On the left is a typical photograph of the separator which exhibits good flexibility and mechanical stability. Fig. 1b and Fig. 1c show SEM and TEM images of the graphene used which shows a crumpled laminar structure and consists of wrinkled sheets with a size of up to 10 μm. Raman spectrum of the graphene is shown in Fig. S1, and a prominent G band at 1581 cm^{-1} and a D band at 1363 cm^{-1} were observed. Because the graphene was produced from graphite through

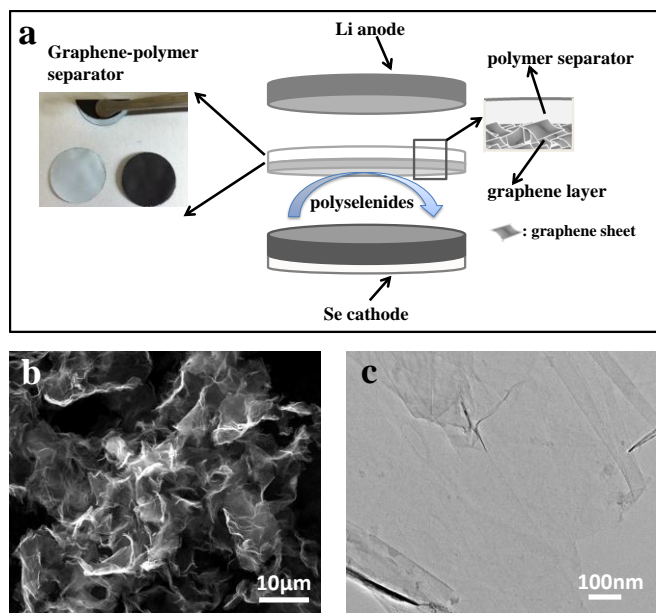an intercalation-exfoliation process without involving oxidation, a

Fig. 1 (a) Schematic configuration of a Li-Se cell with a graphene-polymer separator. The left figure shows a photograph of a graphene-polymer separator with the black side of graphene and the white side of polymer. (b) SEM image and (c) TEM image of the graphene material used for the graphene-polymer separator.

high electrical conductivity and quality were achieved.[26] It is also worth noting that the thickness of the graphene layer is about 5 μm (Fig. S2) and the weight is only 0.3 mg cm^{-2}, much lighter than the active material loaded in the cathode (~4 mg cm^{-2}), which ensures the improved energy density.

The comparison of the discharge voltage profiles of the cells with two different separators during the initial 50 cycles at a 0.5C rate is presented in Fig. 2a and Fig. 2b. Fig. 2a shows the discharge curves of the cell with a graphene-polymer separator, which exhibits two separate plateaus. The upper plateau at 2.15 V corresponds to the reduction of elemental selenium to soluble high-order polyselenides (Li_2Se_x, $3 \leqslant x \leqslant 8$), and the lower plateau at 1.96 V suggests the reduction of soluble polyselenides to insoluble low-order Li_2Se_2/Li_2Se. The multistep phase transitions of the selenium cathode are in agreement with Cui's results using the same electrolyte.[14] Notably, the initial discharge capacity of the cell with a graphene-polymer separator reached 631mAh g^{-1}, 93% of the theoretical value (678mAh g^{-1}), and there is almost no change in the well-retained upper discharge plateau (Fig. 2a). However, Fig. 2b shows continuous capacity degradation in the upper plateau discharge capacity in the cell without graphene, revealing the unique function of graphene in successfully blocking polyselenides.

To demonstrate the issue more clearly, the changes of the upper/lower plateau discharge capacities with different separators are quantified in Fig. 2c and Fig. 2d, respectively. Apparently both the upper plateau discharge capacities and lower plateau discharge capacities of the cell with a graphene-polymer separator remain highly reversible, whereas the upper/lower plateau capacities of the cell without graphene decrease to 29% and 26% of the original values. Generally, the upper plateau region corresponds to the formation of highly soluble polyselenides,[14] therefore, the well-retained upper discharge plateau indicates effectively suppressed polyselenide diffusion to the anode. The lower plateau region corresponds to the formation of solid Li_2Se_2/Li_2Se,[14] where a close contact between polyselenides containing electrolyte and the conductive network is a prerequisite in order to complete the liquid
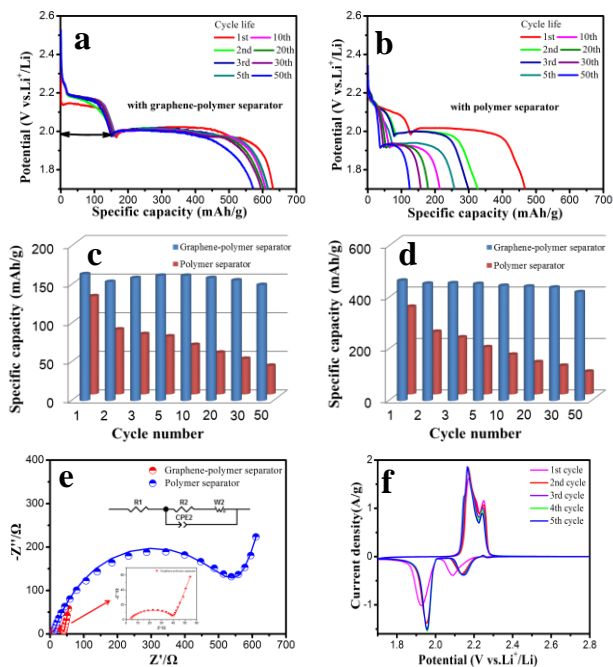

Fig. 2 Discharge curves of Li-Se cells with (a) the graphene-polymer separator and (b) a polymer separator at 0.5C. (c) Upper plateau discharge capacities and (d) lower plateau discharge capacities of Li-Se cells with different separators at 0.5C. (e) Electrochemical impedance spectra of Li–Se cells with a graphene-polymer separator and a polymer separator (inset is the magnified plot for the cell with a graphene-polymer separator). (f) Cyclic voltammograms of the cell with the graphene-polymer separator at 0.1 mV s^{-1} in the potential window from 1.7 to 2.8 V *vs.* Li$^+$/Li.

to solid (Li_2Se_2/Li_2Se) reaction. Therefore, with a graphene-coated layer, the Se cathode maintains high reversibility during cell operation.

Fig. 2e shows electrochemical impedance spectroscopy (EIS) plots of Li-Se cells with and without the graphene-coated separator before cycling. The EIS plots of the electrodes are constituted by a single depressed semicircle in the high frequency region and an inclined line at low frequency. The experimental data are represented as symbols, and the continuous lines are fitted data according to the equivalent circuit shown in the inset of Figure 2e. The elements in the equivalent circuit include Ohmic resistance of the electrolyte and cell components (R_1), charge-transfer resistance (R_2) which represents the electrode reaction kinetics,[27] a constant phase element (CPE_2), and Warburg impedance (W_2). It can be seen that the value of R_2 for the cell with a graphene-polymer separator (38 Ω) is an order of magnitude lower than that for the cell with a polymer separator (507 Ω), revealing a dramatic decrease in the cathode resistance. EIS plots recorded after 10 cycles are shown in Fig. S3, and the cell with a graphene-polymer separator also shows a much smaller impedance semicircle after cycling. The impedance results indicate that the highly conductive graphene works well to reduce the internal resistance of the cathode. Fig. 2f shows cyclic voltammograms (CV) of the cell with a graphene-polymer separator for the first five cycles. The two distinguished cathodic peaks are consistent with the discharge voltage profiles in Fig. 2a. After the first cycle, the two cathodic peaks shift slightly to higher voltages of 1.96V and 2.15V, probably due to an electrochemical activation process involving the rearrangement of active material to more favorable positions.[21] Notably, the cathodic and anodic peaks almost

ChemComm

COMMUNICATION

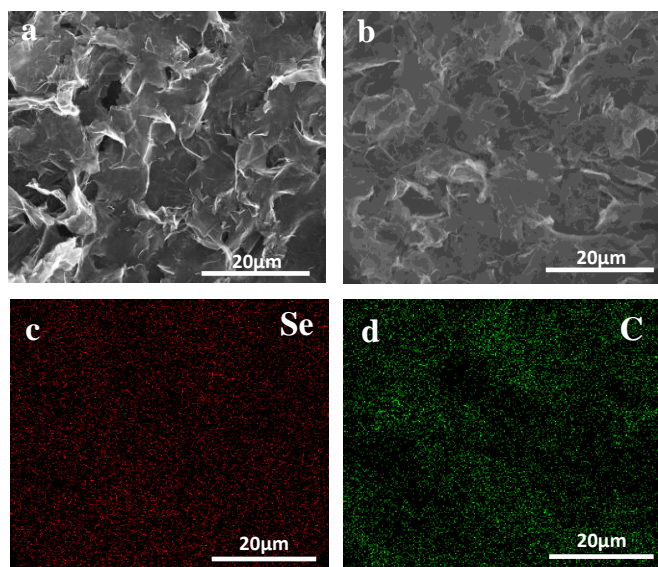remain constant after the first cycle, demonstrating the good

Fig. 3 SEM images of graphene on a graphene-polymer separator (a) before cycling and (b) after 20 cycles. Elemental mapping of (c) selenium and (d) carbon after 20 cycles.

reversibility and stability of the cell. For comparison, the CV curves of the cell without graphene (Fig. S4) exhibit wider peaks and a lower current with large polarization, indicating a slow kinetic process during cycling. Moreover, different from two oxidation peaks in Fig. 2f, there is only one oxidation peak observed in Fig. S4 and it suggests that after the first cycle, the discharge product should be intermediate Se_x^{2-} instead of elemental Se,[14] showing poor reversibility of the cell without graphene.

SEM images of the surface of the graphene-polymer separator before and after cycling are compared in Fig. 3a and Fig. 3b to further verify the effectiveness of the graphene as a good reservoir to accommodate the migrating polyselenides. As can be seen, the surface of the graphene before cycling (Fig. 3a) was highly porous with numerous interconnected and overlapping graphene sheets, which facilitate good electrolyte penetration. After 20 cycles, it shows good structural stability without cracks and large agglomerates (Fig. 3b). This feature is important because it has been reported that the accumulation of active material on the conducting surface may block the electron pathway and result in degraded electrochemical performance.[28] This therefore suggests that the dissolved polyselenides are probably absorbed and stored within the stacked graphene structure rather than diffuse through the polymer separator to the Li anode and cause the shuttle effect. This allows them to be re-used in subsequent cycling and the Coulombic efficiency is also increased. Fig. 3c and Fig. 3d show the elemental Se and C maps of the graphene coating after 20 cycles, suggesting that selenium is distributed homogeneously throughout the graphene layer. Fig. S5 shows a cross-sectional elemental line scan of Se on the graphene layer after cycling. We can see a selenium concentration gradient, where stronger selenium signals are nearer the cathode and weaker signals are on the side of the polymer separator. This further proves that graphene functions well to prevent the polyselenides diffusing to the anode region. Consequently, with respect to the well-retained specific capacity during cycling, the graphene layer plays multiple roles in improving the electrochemical performance: 1) an excellent embedded conductive network in the cathode region to facilitate electron transport and effectively reduce the resistance; 2) an absorption agent to restrict the polyselenide-
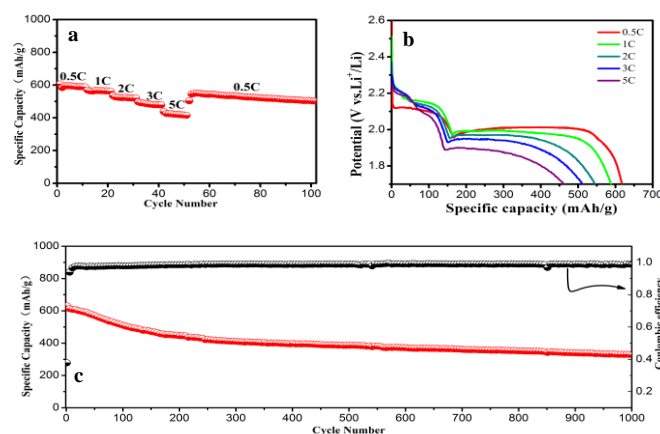

Fig. 4 Electrochemical performance of the Li-Se cell with a graphene-polymer separator. (a) Rate capability at different rates. (b) Discharge profiles at different rates. (c) Cycling stability and Coulombic efficiency at 0.5C for 1000 cycles.

containing electrolyte to the cathode region; 3) a "polyselenide reservoir" to suppress the free diffusion of polyselenides to the anode, resulting in significantly improved stability and reversibility of the electrodes.

The rate capability and cycling stability of a Li-Se cell with a graphene-polymer separator were further investigated, as shown in Fig. 4. The selenium cathode was cycled at different C-rates to evaluate its rate capability and electrode kinetics (Fig.4a). When the C-rate was increased from 0.5C to 1C, 2C, 3C and 5C, the cell was able to respectively deliver 95%, 89%, 83% and 75% of the capacity at 0.5C. Remarkably, even at a high C-rate of 5C, a high reversible capacity of 463 mAh g^{-1} was achieved, which is higher than the reported selenium-based cathodes,[12, 20-22, 24, 25] indicating good conductivity and improved charge transfer kinetics of the cell. Furthermore, a stable discharge capacity of 546 mAh g^{-1} could be recovered when the current density was restored to 0.5C, indicating the good structural stability of the electrode. For comparison, the cell without graphene failed to exhibit electrochemical activity at 3C (Fig. S6). Fig. 4b shows the corresponding discharge profiles at different current densities. Two plateaus were flat and stable even at 5C, suggesting a kinetically efficient process with a small barrier. The cycling stability of the cell with a graphene-polymer separator was investigated at 0.5C for up to 1000 cycles (Fig. 4c), showing exceptional stability. With respect to the initial specific capacity of 631 mAh g^{-1}, the cell retained a reversible capacity of 331 mAh g^{-1} after 1000 cycles, corresponding to an extremely low capacity decay rate of 0.048% per cycle. The average Coulombic efficiency was calculated to be above 98%. In comparison, a selenium cathode without graphene only delivered 86 mAh g^{-1} after 100 cycles (Fig. S7), showing severe capacity loss. The cycling performance at a higher rate of 1C was further tested, as shown in Fig. S8. The excellent performance can be ascribed to the graphene interlayer on the separator that enables adsorption, immobilization, and re-utilization of the active material within the highly conductive graphene layer, and at the same time stabilizes the active material in the cathode region during the long cycle testing. Moreover, the fast transport of electrons and lithium ions during the redox reaction as a result of the presence of graphene was responsible for the superior rate behavior of the electrode.

To further elucidate the electrochemical reaction mechanism of the pure selenium electrode, the structure of the electrode at different charge/discharge states was investigated by XRD and Raman spectroscopy (Fig. S9). The XRD patterns of the pristine selenium cathode indicated a well crystallized structure and showed all the

diffraction peaks corresponding to trigonal Se. After cycling, no diffraction peaks of crystalline Se could be observed, which indicates that, after cycling, the Se in the cathode existed in a non-crystalline state. Raman measurements showed that the pristine cathode exhibited a strong peak at 231 cm^{-1} as evidence of the first-order A$_1$ symmetric bond-stretching modes of trigonal Se,[29] but after the first cycle, a sharp peak at 250 cm^{-1} appeared, which corresponds to the vibration of amorphous chain-structured Se, indicating the formation of disordered Se chains. Similar results have been reported by Guo et al[20, 25] and it is believed that chain-structured Se presents better electrochemical behavior during cycling.

In conclusion, a graphene-polymer dual layer separator was developed to improve Li-Se battery performance with a pure selenium cathode. The graphene not only facilitates electron transport, but also prevents polyselenide migration to the anode region by absorbing and trapping them in the graphene. With the graphene-polymer separator, the pure Se cathode was able to deliver excellent cycling performance up to 1000 cycles with a low decay rate of 0.048% per cycle and superior rate performance up to 5C. We believe the design of a dual structured composite separator shows great promise for further improvements in advanced electrochemical energy storage systems.

Notes and references

Shenyang National Laboratory for Materials Science, Institute of Metal Research, Chinese Academy of Sciences, Shenyang 110016, China.

E-mail: fli@imr.ac.cn

1 M. Armand and J. M. Tarascon, *Nature*, 2008, **451**, 652-657.
2 J. B. Goodenough and Y. Kim, *Chem. Mater.*, 2010, **22**, 587-603.
3 P. G. Bruce, S. A. Freunberger, L. J. Hardwick and J. M. Tarascon, *Nat. Mater.*, 2012, **11**, 19-29.
4 J. M. Tarascon and M. Armand, *Nature*, 2001, **414**, 359-367.
5 J. B. Goodenough and K. S. Park, *J. Am. Chem. Soc.*, 2013, **135**, 1167-1176.
6 D. W. Wang, Q. C. Zeng, G. M. Zhou, L. C. Yin, F. Li, H. M. Cheng, I. R. Gentle and G. Q. M. Lu, *J. Mater. Chem. A.*, 2013, **1**, 9382-9394.
7 A. Manthiram, Y. Z. Fu and Y. S. Su, *Acc. Chem. Res.*, 2013, **46**, 1125-1134.
8 X. L. Ji, K. T. Lee and L. F. Nazar, *Nat. Mater.*, 2009, **8**, 500.
9 G. M. Zhou, S. F. Pei, L. Li, D. W. Wang, S. G. Wang, K. Huang, L. C. Yin, F. Li and H. M. Cheng, *Adv. Mater.*, 2014, **26**, 625-631.
10 F. F. Li, W. Lu, S. Z. Niu and B. H. Li, *New. Carbon. Mater.*, 2014, **29**, 309-315.
11 Q. Zhang, X. B. Cheng, J. Q. Huang, H. J. Peng and F. Wei, *New. Carbon. Mater.*, 2014, **29**, 241-264.
12 J. T. Lee, H. Kim, M. Oschatz, D. C. Lee, F. X. Wu, H. T. Lin, B. Zdyrko, W. I. Cho, S. Kaskel and G. Yushin, *Adv. Energy Mater.*, 2014, DOI: 10.1002/aenm.201400981.
13 C. P. Yang, Y. X. Yin and Y. G. Guo, *J. Phys. Chem. Lett.*, 2015, **6**, 256-266.
14 Y. Cui, A. Abouimrane, J. Lu, T. Bolin, Y. Ren, W. Weng, C. Sun, V. A. Maroni, S. M. Heald and K. Amine, *J. Am. Chem. Soc.*, 2013, **135**, 8047-8056.
15 D. W. Wang, G. Zhou, F. Li, K. H. Wu, G. Q. Lu, H. M. Cheng and I. R. Gentle, *Phys. Chem. Chem. Phys.*, 2012, **14**, 8703–8710.
16 L. Ji, M. Rao, H. Zheng, L. Zhang, Y. Li, W. Duan, J. Guo, E. J. Cairns and Y. Zhang, *J. Am. Chem. Soc.*, 2011, **133**, 18522-18525.
17 W. Y. Li, Q. F. Zhang, G. Y. Zheng, Z. W. Seh, H. B. Yao and Y. Cui, *Nano. Lett.*, 2013, **13**, 5534-5540.
18 Y. S. Su and A. Manthiram, *Nat. Commun.*, 2012, **3**, 1166-1172.
19 G. M. Zhou, L. Li, D. W. Wang, X. Y. Shan, S. F. Pei, F. Li and H. M. Cheng, *Adv. Mater.*, 2014, DOI: 10.1002/adma.201404210.
20 C. P. Yang, S. Xin, Y. X. Yin, H. Ye, J. Zhang and Y. G. Guo, *Angew. Chem. Int. Ed.*, 2013, **52**, 8363-8367.
21 L. Chao, Y. H. Xu, Y. J. Zhu, Y. H. Liu, S. Y. Zheng, Y. Liu, A. Langrock and C. S. Wang, *ACS Nano*, 2013, **7**, 8003-8010.
22 J. J. Zhang, L. Fan, Y. C. Zhu, Y. H. Xu, J. W. Liang, D. H. Wei and Y. T. Qian, *Nanoscale*, 2014, **6**, 12952-12957.
23 Z. Li, L. X. Yuan, Z. Q. Yi, Y. Liu and Y. H. Huang, *Nano Energy*, 2014, **9**, 229-236.
24 K. Han, Z. Liu, J. M. Shen, Y. Y. Lin, F. Dai and H. Q. Ye, *Adv. Funct. Mater.*, 2014, DOI: 10.1002/adfm.201402815.
25 H. Ye, Y. X. Yin, S. F. Zhang and Y. G. Guo, *J. Mater. Chem. A.*, 2014, **2**, 13293-13298.
26 W. C. Ren and H. M. Cheng, *Nat. Nanotechnol.*, 2014, **9**, 726-730.
27 S. S. Zhang, *J. Electrochem. Soc.*, 2012, **159**, A920-A923.
28 H. B. Yao, H. Yan, C. M. Li, G. Y. Zheng, D. S. Kong, Z. W. Seh, V. K. Narasimhan, C. Liang and Y. Cui, *Energ. Environ. Sci.*, 2014, **7**, 3381-3390.
29 I. L. Li, J. P. Zhai, P. Launois, S. C. Ruan and Z. K. Tang, *J. Am. Chem. Soc.*, 2005, **127**, 16111-16119.